Lab on a Chip

PAPER

View Article Online
View Journal | View Issue

Cite this: *Lab Chip*, 2026, **26**, 2061

A portable, low-cost, point-of-care DNA amplification kit with impedance-based detection for decentralized antimicrobial resistance diagnostics

Koosha Karimi, [a] Miriam Arroyo, [b] Erin E. Chille, [b] Timothy G. Stephens, [b] Donal Barrett, [c] Vicent Pelechano, *[c] Debashish Bhattacharya *[b] and Mehdi Javanmard*[a]

This study introduces a low-cost, portable DNA amplification kit that performs a modified loop-mediated isothermal amplification (LAMP) reaction, which produces DNA nanoballs and combines it with a previously developed microfluidic impedance-based digital assay to deliver a potential all-in-one, point-of-care (POC) diagnostic platform for the detection of target nucleic acids. The device combines sample processing and detection in a single streamlined workflow, utilizing induction heating and Arduino-based temperature control, along with several engineering innovations, including a custom-designed polycarbonate microtube holder and an optimized thermocouple-based temperature-control feedback system, ensuring stable reaction conditions for reproducible amplification. System performance was validated through the detection of a synthesized β-lactamase target DNA gene block, including samples with additional non-target background DNA. In addition to a qualitative colorimetric readout, label-free impedance-based quantification confirmed the robust production of DNA nanoballs with high specificity and minimal background interference. The amplification quality was revealed to be comparable to that of a commercial thermal cycler. Subsequent sensitivity testing using serial dilutions of the target DNA (between 10^1–10^5 copies per μl) in a complex background DNA mixture demonstrated detection results that strongly correlated with quantitative PCR (qPCR). These findings demonstrate that the amplification kit achieves performance parity with gold-standard nucleic acid detection methods while offering portability, affordability, and ease of use. By enabling accurate, rapid, and decentralized diagnostics without reliance on laboratory infrastructure, this combined workflow holds promise for advancing infectious disease monitoring and antimicrobial resistance surveillance, among other applications, at the point of care.

Received 21st January 2026,
Accepted 18th February 2026

DOI: 10.1039/d6lc00062b

rsc.li/loc

I. Introduction

Antimicrobial resistance (AMR) is part of an escalating global issue, named the largest global health threat by the World Health Organization, and is predicted to cause 10 million deaths annually by 2050 if left unaddressed.[1,2] Medical approaches for the detection of AMR currently include culturing and isolation techniques in which pure cultures are tested for AMR capabilities. However, these techniques are time and labor-intensive and can limit patient care timelines; therefore, molecular-based diagnostics have been increasingly utilized for the rapid and reliable detection of AMR.[3] Currently, protein-based methods, such as lateral flow tests, have limited use for AMR detection; these tests are constrained by the need to develop antibodies, which add a layer of difficulty to the diagnostic development process and limit their use to high-abundance proteins.[2,3] Nucleic acid-based diagnostics, on the other hand, do not require culturing, have high sensitivities, intrinsic target flexibility, and amplification capabilities that allow for earlier detection, and thus are preferred over traditional culture or protein-based diagnostics.[4] There are also currently established workflows of using nucleic acid detection for pathogen monitoring, *i.e.*, SARS-CoV-2.[5–7]

Thus, the focus of this study lies in developing a tool for nucleic acid-based AMR detection, aligning with other recent studies that emphasize the importance of point-of-care

[a] *Department of Electrical and Computer Engineering, Rutgers, The State University of New Jersey, USA. E-mail: mehdi.javanmard@rutgers.edu*
[b] *Department of Biochemistry and Microbiology, Rutgers University, New Brunswick, New Jersey, USA. E-mail: d.bhattacharya@rutgers.edu*
[c] *SciLifeLab, Department of Microbiology, Tumor and Cell Biology, Karolinska Institutet, Solna, Sweden. E-mail: vicente.pelechano.garcia@ki.se*

diagnostics in curbing AMR's spread by enabling faster on-site identification of resistant pathogens.[8] In this study, β-lactamase genes were of interest, which confer resistance to microbes from β-lactam antibiotics by hydrolyzing the antibiotic's β-lactam ring, rendering them ineffective. β-lactamase genes are increasingly found in pathogens such as *Escherichia coli* and *Klebsiella pneumoniae* and are of growing concern worldwide.[9,10]

Real-time quantitative polymerase chain reaction (qPCR) stands as the gold standard for both the detection and quantification of nucleic acids. However, various other nucleic acid-based methods have been devised and increasingly utilized.[4] Isothermal amplification (IA) techniques require simple hardware and are rather insensitive to polymerase inhibitors, making the amplification process robust.[11] The most promising IA techniques for use in microfluidic devices include nucleic acid sequence-based amplification (NASBA),[12] recombinase polymerase amplification (RPA),[13] helicase-dependent amplification (HDA),[14] and loop-mediated isothermal amplification (LAMP).[15] LAMP stands out among the isothermal amplification techniques because of its straightforward implementation and adaptability. Due to its low operational costs and the simplicity of its hardware, LAMP is considered one of the most promising techniques for genetic analysis in resource-constrained environments, as there is no need for a thermal cycler and has lower reagent consumption than other techniques.[11,16] The method couples 4–6 oligonucleotide primers targeting a region of interest with a strand-displacing polymerase that results in large multi-stem–loop DNA structures, due to annealing between alternately inverted repeats in the primers.[15] Quantification of the reaction can then be accomplished using a variety of methods, including gel electrophoresis, fluorescent, and colorimetric techniques.[4,16,17]

Although there are established quantification methods for LAMP amplification that are effective, some methods, such as the use of fluorescent chemicals, can raise reagent costs and require complex analysis systems or specialized platforms for sample detection and readout that limit the integration feasibility.[18,19] On the other hand, colorimetric methods offer a simpler solution by indicating H+ ion production through a visible reagent color change. However, this approach is prone to false positives, particularly with acidic samples, such as raw saliva, which may require additional neutralization steps before testing.[20,21] Therefore, the development of simplified, yet accurate, detection methods for nucleic acid amplification is highly desirable. One alternative is electrochemical detection, which measures impedance changes and provides a label-free solution to DNA amplification detection. In our group's previous study, Tayyab *et al.* developed a simplified one-pot isothermal amplification method for nucleic acids that detects changes in electrical impedance.[22] By incorporating two compaction primers, which are complementary to a common region in the amplicons, the modified LAMP reaction allows for self-nucleation of amplified DNA into "nanoballs".[22] By applying an excitation voltage at specific frequencies, the impedance response of the material is recorded, and the presence or absence of the material can be detected.[23] The formation of DNA nanoballs provides several key merits relevant to this work. First, their compact size and high molecular density produce a strong, discrete impedance perturbation when traversing the microfluidic channel between electrodes, enabling label-free, digital electrical detection without the need for fluorescent dyes or beads. Moreover, because these DNA nanoballs form directly during amplification (LAMP) in a single-pot reaction, they enable seamless coupling of isothermal amplification with downstream impedance-based quantification, supporting a simplified, low-cost, and portable diagnostic workflow. This detection assay provides a method for quantifiable, label-free measurement of DNA or RNA targets, such as pathogens including SARS-CoV-2 and HIV, with an established sensitivity of down to 10 copies per sample.[22] This detection method offers a label-free, sensitive, and cost-effective alternative to standard PCR techniques.[24]

In most nucleic acid diagnostic devices, the sample treatment (processing) and the testing (detection) stages are separate, which adds time and complexity to the analysis. The reason for this separation stems from differences in requirements for each stage. The sample treatment stage includes nucleic acid extraction, purification, and amplification, which typically require specialized reagents, precise temperature control, expensive lab equipment, and optimized protocols. The sensitivity and specificity of nucleic acid detection methods heavily rely on the efficiency of sample preparation and processing; any compromise in these stages could lead to false results or missed diagnoses. Biosensors, which are often based on principles such as fluorescence and electrochemistry for the detection stage, require very stable conditions to achieve high precision and low levels of background noise. Therefore, integrating the two stages of sample processing and detection would necessitate intricate engineering to harmonize their distinct requirements.

Here, we present an automated programmable heating apparatus that will eliminate the need for complex and expensive lab equipment (*e.g.*, commercial thermal cyclers) by performing the modified LAMP reaction, which self-nucleates the amplified target DNAs into nanoballs that can be subsequently detected by our group's previously established device; a simple, inexpensive, electrical impedance-based detection system.[22] This combined workflow streamlines sample processing and detection, expanding the functionality of the microfluidic digital assay and enabling end-to-end processing for target nucleic acid detection. Thus, the DNA amplification kit presented in this paper, combined with the microfluidic digital assay, addresses the aforementioned deficiencies in standard isolated methods, with the eventual goal of integrating both systems into a portable, affordable, all-in-one device that offers a novel method for detecting genes without requiring extensive laboratory infrastructure. In this study, we utilized β-lactamase genes to validate the device's ability to accurately detect AMR genes and demonstrate the system's potential utility in rapid diagnostic applications for

AMR. This aligns with efforts to address AMR at the point of care, which are essential for effective containment and targeted treatment strategies in both community and hospital settings. However, this workflow is not limited to β-lactamase gene or AMR detection, with inherent flexibility for use in the detection of any DNA/RNA targets (SARS-CoV-2, HIV, *etc.*) with known regions of interest.

II. Methods and materials

A. Protocol for using the amplification kit with the impedance-based microfluidic digital assay for DNA nanoball production and detection

Fig. 1 presents the high-level system flowchart that illustrates the full, meticulous diagnostic platform's protocol, utilizing the amplification kit for the LAMP reaction alongside the impedance-based microfluidic device for DNA nanoball detection. This application-specific heating module, designed to facilitate the production of DNA nanoballs (DNA amplification), is combined into the impedance-based detection system, thereby consolidating the sample processing and detection stages into a single, decentralized, cohesive workflow. Following the amplification stage, the generated DNA nanoballs can be evaluated and detected using the impedance-based electrical detection system[22] (see Fig. 4).

B. Induction heating

Induction heating is a technique employed to heat electrically conductive materials, such as metals and semiconductors, through electromagnetic induction. This process generates an alternating current (AC) within an inductor coil, creating an electromagnetic field that penetrates the target material and induces eddy currents, as shown in Fig. 2. These currents interact with the material's internal resistance, producing Joule heating, which increases the temperature internally rather than relying on external heat sources. Induction heating offers several advantages, including rapid and contactless heating. This can be ideal for various applications in manufacturing and diagnostics, including heat treatment, melting, and brazing, due to its ability to achieve high temperatures quickly and efficiently.[25,26]

In our DNA amplification kit, induction heating is employed to maintain the optimal temperature required for the LAMP reaction. By incorporating a K-type thermocouple temperature sensor and an Arduino-controlled feedback loop, the system ensures precise temperature control, which is critical for the sensitive reactions involved in nucleic acid amplification. This setup allows for rapid heating, minimized temperature fluctuations, and effective energy use, aligning with the requirements for a portable, point-of-care diagnostic device. Another noteworthy advantage of induction heating is its safety, as it selectively heats conductive materials without affecting non-conductive objects such as human skin, making it user-friendly and suitable for operators with minimal or no training or laboratory experience. Operators are protected from accidental burns or injuries, and the non-contact nature of induction heating further enhances its safety, eliminating risks associated with traditional heating methods involving open flames or direct electrical contacts. These characteristics reduce the need for extensive operator training, making induction heating accessible even to those without specialized laboratory skills.[25,26]

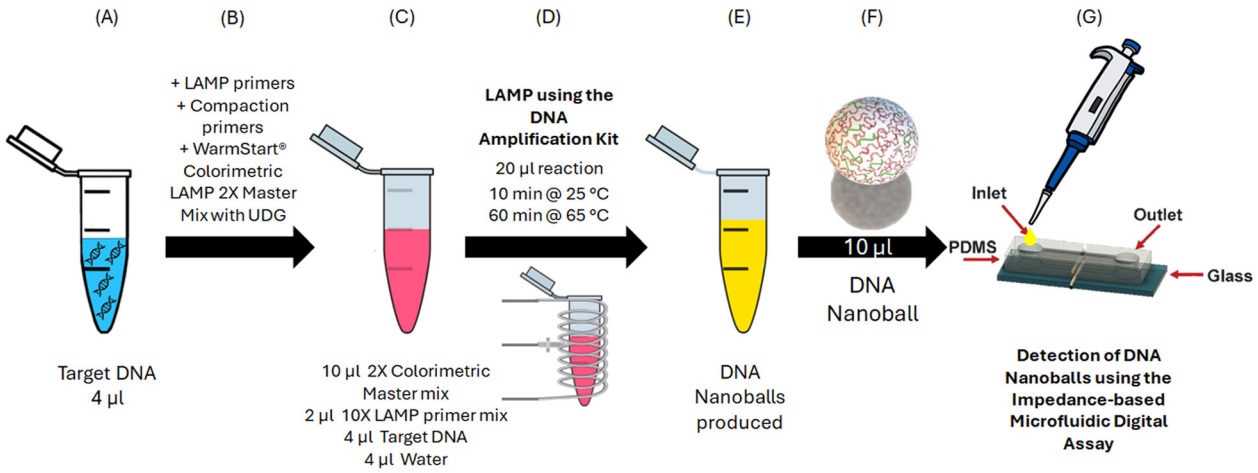

Fig. 1 High-level system diagram outlining the diagnostic platform's workflow from sample processing utilizing the portable DNA amplification kit, performing the LAMP reaction and producing the DNA nanoballs, followed by the microfluidic impedance-cytometer-based digital assay for detection of the formed DNA nanoballs. (A) Sample processing begins with a microtube containing 4 µL of target DNA (in the positive sample case, β-lactamase genes). (B) The primers and the WarmStart Colorimetric LAMP 2× Master Mix are added to produce (C) the final red-colored, ready-to-be-amplified 20 µl solution. (D) The DNA amplification kit performs the modified LAMP reaction at the specified conditions on the sample to produce the DNA nanoballs. (E) The amplified solution will turn yellow if it contains target DNA as the pH changes due to the production of the DNA nanoballs. This is the first benchmark for visually and qualitatively evaluating the production of (F) DNA nanoballs. (G) Lastly, using a pipette, a 10–15 µl drop of the solution undergoes electronic readout detection *via* the impedance-cytometer-based microfluidic digital assay explained in section II. G and illustrated in Fig. 4.

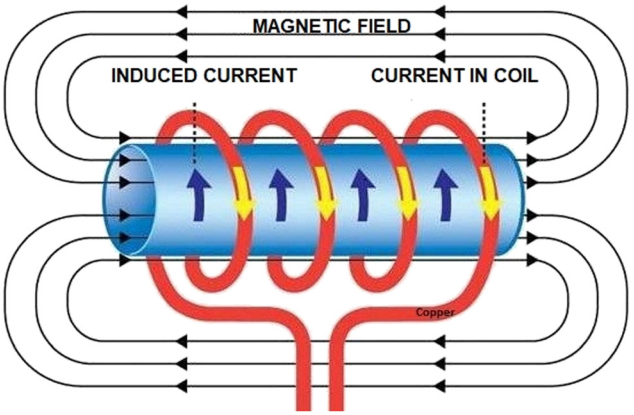

Fig. 2 Basic principle of induction heating.[26]

C. Automated programmable DNA amplification kit circuit design

The intricate circuit configuration of the DNA amplification kit is depicted in Fig. 3(A). The reactants (described in section II: H. modified LAMP for DNA amplification) are added to an Eppendorf microtube, which is subsequently placed within our specifically designed microtube holder. The holder is fabricated from a heat-resistant 3D-printing material, as elaborated on in the following section. A copper coil, connected to a zero-voltage-switching (ZVS) low-voltage induction-heating module, is positioned around the microtube. A K-type thermocouple temperature sensor is situated between the coil turns to continuously monitor the temperature of the microtube, relaying the data to an Arduino Mega microcontroller *via* a MAX6675 amplifier. This amplifier enhances the temperature signal obtained from the vicinity of the microtube and transmits it to the SPI serial interface ports of the microcontroller (SCK, CS, SO). The temperature readings are continuously displayed on a 2 × 16 LCD screen. This feedback loop is vital, as it determines whether the heating process should continue or whether the target temperature has been reached. The programmed microcontroller makes this determination and subsequently regulates the ON or OFF state of the system using a 5 V one-channel relay module, which controls the connection between the 10 V DC power supply and the ZVS heating module.

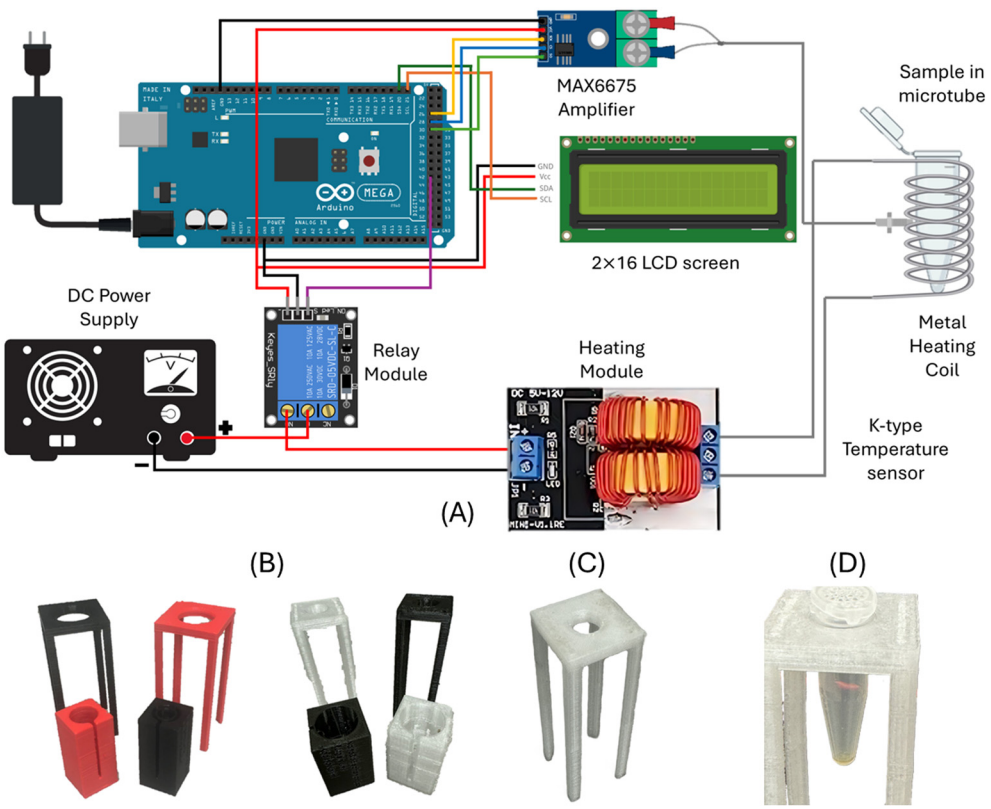

Fig. 3 Electronic circuit configuration and progression of microtube holder prototypes for the DNA amplification kit. (A) Elaborated circuit schematic of the Arduino-controlled heating apparatus. The setup includes an Arduino mega microcontroller connected to a MAX6675 amplifier to read temperature data from a K-type thermocouple, which measures the temperature at the metal heating coil, which is wrapped around a microtube containing the sample. A relay module, controlled by the Arduino, switches the DC power supply on and off to regulate the heating module. The real-time temperature is displayed on a 2 × 16 LCD screen, allowing precise control of sample heating. (B) Prototype microtube holders printed in box and footstool designs using various heat-resistant materials (with different colors indicating distinct printing filaments). (C) The finalized footstool-shaped microtube holder was fabricated from polycarbonate (PC). (D) The post-LAMP reaction color-shifted microtube reactants positioned in the custom-designed microtube holder.

D. Design and material selection of a heat-resistant microtube holder for the modified LAMP reaction

The purpose of the microtube holder is to maintain separation between the metal coil and the microtube, as the elevated temperatures reached during the LAMP reaction could potentially deform or melt the microtube upon contact. The holder design needed to ensure that neither the microtube nor the holder itself made contact with the metal coil to prevent such deformation or melting. Additionally, it was necessary for the microtube to remain visible to monitor the reaction solution's color change, which serves as an essential indicator of system functionality.

Several design prototypes were tested, with two primary options highlighted in Fig. 3(B): the "box" and the "footstool". The box design featured a central hole sized to fit the metal coil, with a circular structure supported by four columns to secure the microtube. However, this design had two limitations: the microtube was obscured during experiments, and the structure posed challenges for 3D printing. Consequently, the footstool design (Fig. 3(C)) was developed to address these issues while fulfilling the same purpose.

Once the design was finalized, the next critical criterion was identifying a heat-resistant 3D printing filament capable of withstanding temperatures around 150 °C. Fig. 3(B) displays prototypes printed in various materials, each with distinct thermal resistance properties, as summarized in Table 1. In addition to heat deflection temperature (HDT), factors such as cost, availability, printability, and the need for annealing were considered. Annealing, a post-printing process that increases the strength and heat resistance of printed objects, involves reheating to or just above the glass transition temperature (T_g) but below the melting point. Although annealing enhances durability, it also leads to shrinkage along the X, Y, and Z axes, which complicates the fabrication of delicate, accurately sized components. Certain filaments listed in Table 1, such as ONYX, require specialized conditions for successful printing. Others have low HDT or are expensive. For practicality, a filament that does not require annealing, is affordable, readily available, and has an HDT exceeding 100 °C (sufficient for running the LAMP reaction at the maximum temperature of 65 °C inside and around 90 °C outside the microtube as measured during operation) was preferred. According to Table 1, enriched with manufacturer data (as of January 2026), polycarbonate (PC) has all the desired characteristics.[32] Ultimately, the footstool design, fabricated from PC filament, was selected as the final choice for the microtube holder.

E. Microcontroller programming and voltage optimization

The microcontroller plays a pivotal role in regulating the operation of the ZVS heating module by managing the ON/OFF states based on real-time temperature feedback from a K-type sensor. This feedback determines whether the relay module, which bridges the power supply to the ZVS heating module, is activated. Initially, essential libraries are included to enable proper interfacing with the MAX6675 amplifier and the LCD screen. Following this, key parameters are defined: the digital pin on the Arduino that controls the relay module, variables representing the desired temperature range for the microtube, and the designated DO, CS, and CLK pins on the MAX6675 amplifier. The next step was to call the MAX6675 function to integrate the K-type thermocouple temperature sensor and amplifier, along with the LCD function to connect the 2 × 16 LCD screen to the microcontroller.

Subsequently, initial configurations were implemented, including SPI pin configurations, LCD screen configurations, and a short delay to stabilize the amplifier. Finally, the core of the program was written using a "for" loop that continuously receives temperature readings from the sensor to determine the relay module's activation state. This loop ensures the microtube temperature consistently remains within the target range and displays the current temperature on the LCD screen. A critical delay was embedded in this loop to allow the amplifier sufficient time to gather accurate temperature data before each read cycle, ensuring the reliability of the temperature feedback sent to the microcontroller.

To fine-tune the system's performance, several voltage levels within the 5–12 V range (the operational input range of the ZVS heating module) were evaluated. Higher voltages accelerated the heating rate of the microtube but also led to greater temperature overshoot, reducing accuracy. Conversely, lower voltages minimized temperature overshoot but slowed down the time required for the microtube to reach the target temperature. Balancing these factors, a 10 V setting was selected for the DC power supply, achieving an optimal compromise between heating speed and temperature control precision.

F. K-type temperature sensor placement optimization and calibration for accurate LAMP reaction control

A primary challenge for designing this system was identifying the optimal placement for the temperature sensor. Three configurations were evaluated: placing the sensor directly in

Table 1 Common 3D printing materials and their key characteristics

3D printing filament	PLA[27]	Engineering PLA[28]	PLA+[29]	PETG[30]	ONYX[31]	PC[32]
Heat deformation temperature (HDT)	~60 °C	~95 °C	70–80 °C	70–80 °C	165 °C	111 °C
Cost per kilogram (as of January 2026)	$10–$30	$25–$50	$15–$35	$20–$40	$150–$300	$30–$80
Post-annealing requirement	Required	Required	Not required	Not required	Required	Not required

the solution, positioning it in the empty space inside the microtube just above the solution, or situating it outside and adjacent to the microtube. The first option was ruled out due to two main issues: direct contact between the sensor and reactants was undesirable, and drilling a hole in the microtube lid for sensor insertion would introduce contamination risks. Additionally, frequent RNase decontamination of the sensor tip would be required after each experiment. The second idea addressed the contamination issue, but still necessitated precision drilling in the lid. Ultimately, the third configuration proved ideal, as it avoided all prior issues, especially by eliminating the risk of aerosol contamination as there is microube lid is closed and intact. However, it introduced a new challenge: understanding the correlation between the solution temperature inside the microtube and the external temperature where the sensor was positioned. Notably, this sensor placement closely resembles that used in commercial thermal cyclers, which also detect the temperature in an empty well as a reference for all adjacent wells containing microtubes.[33]

After extensive experimentation, the optimal sensor placement was established within the narrow air gap between the microtube and the metal coil, along with a programmed temperature interval of [64, 66 °C] in the Arduino. With this configuration, there is no risk of aerosol contamination because the microtube is sealed until the end of the LAMP reaction, and the WarmStart Colorimetric LAMP 2× Master Mix with UDG incorporates a uracil-DNA glycosylase system specifically designed to mitigate carryover contamination. These trials highlighted the nonlinear relationship between the external sensor reading and the solution temperature, which led us to the aforementioned temperature interval. Furthermore, the power supply voltage directly influences this temperature correlation and was therefore carefully considered when setting the interval in the Arduino code. With the specified temperature range and a 10 V power supply, a stable microtube temperature of 65 ± 1 °C was achieved, meeting the conditions necessary for the LAMP reaction to proceed smoothly and effectively. This ±1 °C temperature stability of the DNA amplification kit (measured and displayed by the temperature sensor utilized in the DNA Amp Kit) ensures a smooth and unbothered LAMP reaction, comparable to the temperature accuracy of a commercial T100 thermal cycler, which is approximately ±0.5 °C of the programmed target.[34]

G. Digital impedance-based assay for detection of clinical pathogen using DNA nanoballs

The second stage of the overall diagnostic workflow involves electrical detection of the amplified nucleic acids. In our group's previous work, Tayyab *et al.* developed a simplified, one-pot isothermal amplification strategy that enables label-free electrical detection of nucleic acids without the need for external nucleation agents such as microbeads.[22] By introducing "compaction oligonucleotides" into a modified LAMP reaction, amplified DNA self-assembles into compact, three-dimensional, spherical structures referred to as "DNA nanoballs", which are well-suited for electrical detection *via* impedance measurements.

In the present study, our previously described impedance-based detection device by Tayyab *et al.* is employed to evaluate the performance of the DNA amplification kit. As previously reported, DNA nanoballs generated during the modified LAMP process are detected as discrete impedance perturbations as they traverse a microfluidic channel (fabricated from polydimethylsiloxane (PDMS) bonded to a glass substrate) perpendicularly positioned over a pair of gold electrodes patterned onto the glass substrate (Fig. 4(A)) connected to an electronic readout system.[22,35] The microfluidic channel operates *via* passive, capillary-driven flow, thereby eliminating the need for external pumps, tubing, or other complex fluidic control components. This electrical detection scheme, illustrated in Fig. 4(C), provides a quantitative and portable method for assessing amplification efficiency and serves as the downstream readout module for the DNA amplification kit presented here. Specifically, as depicted in Fig. 4(B), when a nanoball occludes the current path and electric field between the electrodes, it causes a detectable spike in impedance, and the number of DNA nanoballs present in the sample can be measured. Fig. 4(C) demonstrates the overall circuit diagram of the electronic readout system. The gold electrodes on the microfluidic chip are connected to a commercial bench-top impedance spectroscope (Zurich Instruments, HF2IS). To

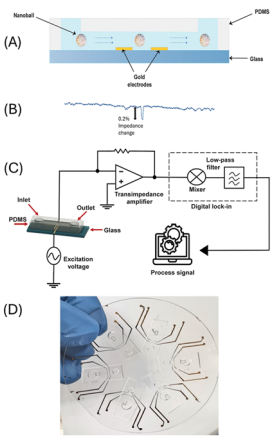

Fig. 4 Electrical detection of DNA nanoballs. (A) Illustration of the passive flow of DNA nanoballs within a microfluidic chip composed of PDMS on a glass substrate, which is integrated with gold electrodes. (B) The transit of DNA nanoballs through the gold electrodes obstructs the current pathway and disrupts the electric field established between the electrodes which in turn generates a spike in the system's impedance response that is recorded as the presence of a single DNA nanoball. (C) Schematic representation of the electronic readout system designed for the microfluidic chip with integrated gold electrodes. (D) Photograph of the 3-inch fused silica wafer containing six sets of electrodes and channels. Each set can be used separately for different samples, simultaneously, or one at a time. From ref. 22, modified with permission under Creative Commons CC-BY license.

minimize noise and interference, the chip was placed inside a Faraday cage in addition to using the digital lock-in amplifier. An excitation voltage can be applied across the electrodes at a programmable frequency. One electrode is directly connected to the impedance spectroscope, while the other is linked to a transimpedance amplifier (Zurich Instruments, HF2TA) with a programmable transimpedance gain. The output from the transimpedance amplifier is fed back into the impedance spectroscope for signal demodulation and filtering, and noise removal. The impedance spectroscope's parameters were optimized with an excitation voltage of 5 V at 5 MHz, a transimpedance gain of 1 kΩ, and a bandwidth (low-pass filter cutoff frequency) of 100 Hz. The signals are stored on a PC and processed using MATLAB software[22] (Fig. 4(C)).

The data from the measurements was processed using an algorithm implemented in MATLAB. The output from the impedance spectroscope typically contains baseline voltage and drift. First, the baseline signal was calculated using a moving average filter, which was then subtracted from the original data to produce a normalized signal that highlights only peaks or spikes. These peaks indicate brief impedance changes caused by a nanoball passing through the microfluidic chip between the electrodes. The signal was then filtered to eliminate background noise, and a threshold was applied to detect peaks. The threshold was set at 2 μV above the noise level. Noise was calculated from variations in the control group's response when no nanoball peaks were present. Afterward, outliers were removed from the peaks, and the number of peaks detected corresponds to the number of nanoballs identified by the system.[22]

H. Modified LAMP for DNA amplification

In our study, the loop-mediated isothermal amplification (LAMP) reaction was optimized to enable efficient amplification of the target DNA at a constant temperature, providing a simpler alternative to conventional PCR. The LAMP reactions were prepared in 20 μL volumes on ice in either Safe-Lock 1.5 mL tubes (Eppendorf, Hamburg, Germany) or standard clear PCR tubes (Avantor, Radnor, PA, USA). Each reaction contained.

10 μL of WarmStart Colorimetric LAMP 2× Master Mix with UDG (New England Biolabs, Ipswich, MA, USA), 2 μL of a 10× LAMP primer mix, 4 μL of the sample (either a synthetic β-lactamase DNA gene block or nuclease-free water for negative controls), "dirty" samples also included 1 μL of methylated mouse DNA standard (Zymo Research, Irvine, CA, USA) as nucleic acid background, and finally nuclease-free water was added to reach 20 μl total for each reaction. The 10× primer mix included 2 μM F3-5′-6-FAM, 2 μM B3, 16 μM FIP, 16 μM BIP, 4 μM LF, 4 μM LB, as well as 2uM LF and 2uM LB compaction oligos.[22]

The LAMP protocol involved two stages: an initial incubation at 25 °C for 10 minutes, followed by amplification at 65 °C for 60 minutes. This temperature profile has been successfully used in various applications for rapid pathogen detection and is particularly effective in resource-limited settings due to its minimal equipment requirements.[5,6] These steps are programmed into our amplification kit.

I. Experimental setup and validation of the DNA amplification kit performance through comparative amplification treating

To validate the system's performance, there were two major test phases; the first was to test the specificity of the DNA amplification using two different heating methods, a traditional thermal cycler and our heating apparatus. The second phase was to determine the sensitivity of the DNA amplification kit compared to the qPCR gold standard method. All of the comparative tests involved the amplification of a target DNA gene block of a β-lactamase AMR gene using the primer mix described above, while the "dirty" samples involved additional methylated mouse DNA standard as nucleic acid background (to test for non-template binding or matrix interaction effects).[8]

As depicted in Fig. 1(A–C), the β-lactamase gene block or nuclease-free water was added to 1.5 mL Eppendorf microtubes, each also containing the 10× LAMP primer mix, and WarmStart Colorimetric LAMP 2× Master Mix with UDG. The positive samples contained the target β-lactamase DNA, while the negative samples contained only nuclease-free water instead. The LAMP master mix includes a visible pH indicator for rapid and convenient detection of LAMP reactions, which should change color only in positive samples due to amplification of the target DNA. Here, we introduce another variation in samples: "pure" samples that contain only the target β-lactamase DNA, and "dirty" samples that contain both the target DNA as well as non-target methylated mouse DNA standard, at 12.5 copies per μL, in the final reaction volume. The mouse DNA standard was chosen because the β-lactamase gene is naturally found only in microbes; thus, the chance of a false-positive signal is very low compared to bacterial DNA standards, which are not guaranteed to be free of this gene. For the initial specificity phase, there were 4 sample groups: dirty negative, dirty positive, pure negative, and pure positive.

To verify the specificity of the amplification reaction using our heating apparatus compared to a commercial Bio-Rad T100 thermal cycler, for each sample group, two identical reactions were prepared for each replicate of the four sample groups. One was made in a PCR tube and placed in the T100 thermal cycler, while the other was made in an Eppendorf tube and placed in our DNA amplification kit. As previously discussed, the negative control samples substituted the target DNA with nuclease-free water as the primary sample component. In order to verify the accuracy of the results, each sample group was performed in triplicate. In the end, all samples were tested using the impedance-based detection system. In this way, the comparison of results (peak counts) from each sample group's microtubes, run on the two heating devices, will determine whether our heating apparatus functions as intended, demonstrating its performance consistency alongside a commercial thermal cycler. Alongside this assessment, we tested whether the

amplification and nanoball formation performance were similar in the presence or absence of non-target "dirty" DNA introduced as background, to ensure that the system is applicable to real-world samples that will contain both target and non-target nucleic acids.

Next, in the sensitivity phase, dirty negative samples with no β-lactamase DNA were run alongside dirty positive samples with various concentrations of the β-lactamase DNA (from 10^1 to 10^5 copies per μL in the final reaction volumes) but a fixed concentration of the non-target mouse DNA (12.5 copies per μL in the final reaction volume). Due to the length of the mouse DNA standard compared to the β-lactamase gene block, the total mass of mouse DNA was always greater than the gene block, even in the most concentrated target samples. In order to compare and verify the sensitivity of our DNA amplification kit, samples were also tested with qPCR as the gold standard method. Similar to what was done in the specificity phase, each sample type was prepared in triplicate, but here, the average cycle thresholds of the triplicates were calculated. The samples that underwent amplification using our heating apparatus were again tested using the impedance-based detection system, while their technical replicates were tested using a StepOnePlus qPCR machine.

J. Real-time quantitative polymerase chain reaction (qPCR)

As stated above, the sensitivity of our amplification kit was tested by comparing the results (peak counts) of each LAMP sample to the gold standard qPCR method. Each sample contained 10 μL of Power SYBR Green PCR Master Mix (Applied Biosystems, Carlsbad, California, USA), 2 μL of 5 μM primer stocks, 5 μL of either the β-lactamase gene block or nuclease-free water if a negative sample, 1 μL of the mouse DNA standard (12.5 copies per μL in the final reaction volume) and the reaction was topped to 20 μl using nuclease-free water. The same sample concentrations were run here as in the DNA amplification kit, from 0 copies per μL to 10^5 copies per μL in the final reaction volume for the β-lactamase gene block, and again each sample was prepared in triplicate. However, in order to adhere to the protocol of the qPCR method, only one pair of primers was used, F3-5′-6-FAM and B3, which span the length of the β-lactamase gene block. In order to create a standard curve to compare the samples to, reactions with the same range in concentration of the β-lactamase gene block were created, with the only difference being that they did not contain any mouse DNA standard DNA and were "pure" samples. The qPCR reactions were run on a StepOnePlus with 35 cycles and an annealing temperature of 62 °C, optimized for the F3/B3 primer pair based on GC percentage. The determined cycle threshold value trend was then compared to the trend of nanoball formation using our DNA amplification kit.

III. Results

The performance of the portable DNA amplification kit was systematically evaluated through a series of validation experiments designed to establish its reliability, specificity, and sensitivity, as well as to benchmark its functionality against established gold-standard techniques. The outcomes of these evaluations confirm that the device provides amplification results consistent with those obtained from commercial thermal cyclers and standard qPCR, while additionally offering portability, cost-effectiveness, and compatibility with impedance-based detection.

The first qualitative benchmark of the amplification process was the colorimetric shift observed in the WarmStart Colorimetric LAMP 2× Master Mix with UDG, which is based on the release of protons during DNA synthesis. In all experiments, positive samples displayed a clear and reproducible transition from red to yellow upon completion of the LAMP process (Fig. 5) while negative samples did not display this color change. This visual output was evident in both "pure" samples, which contained only target β-lactamase RNA, as well as in "dirty" samples, in which target DNA was mixed with excess non-target mouse DNA. By contrast, both negative control groups (pure and dirty negatives) consistently retained their

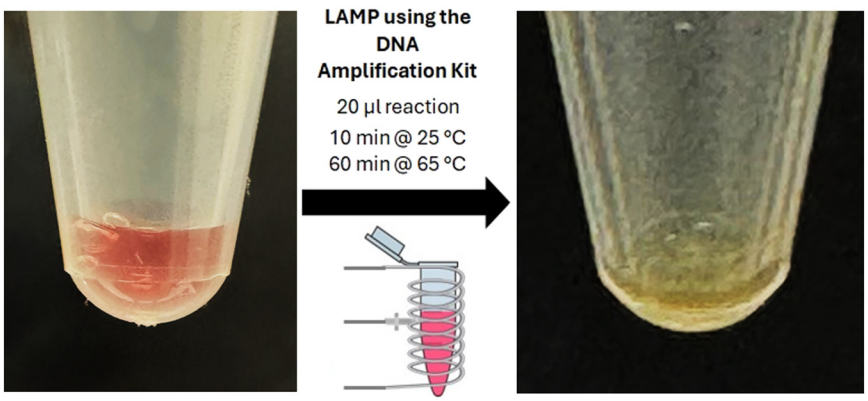

Fig. 5 Color transition from red to yellow observed at the completion of the LAMP reaction for positive samples, attributed to the formation of DNA nanoballs, releasing H^+ ions, and affecting the WarmStart Colorimetric LAMP 2× Master Mix with UDG.

original red color, indicating the absence of amplification. This visual outcome, although qualitative in nature, provides an immediate and accessible measure of reaction success and demonstrates the suitability of the amplification kit for rapid readout in point-of-care settings.

To quantitatively validate the colorimetric shift observations, all amplified samples were subsequently analyzed using the previously described and established impedance-based microfluidic digital assay, which detects the passage of DNA nanoballs through a microfluidic channel as discrete peaks in the impedance signal. Fig. 6(A) illustrates a 7-second window, chosen at random, depicting impedance responses of the detection system in which the signal peaks represent the passage of individual DNA nanoballs through the microfluidic channel. Positive samples treated with the DNA amplification kit or the commercial thermal cycler both demonstrate distinct peaks, whereas the negative control shows minimal peaks, confirming the absence of DNA nanoballs. The impedance responses, processed through a MATLAB-based post-processing algorithm previously discussed in section II. G, align closely between the DNA amplification kit and the thermal cycler, demonstrating the robustness of our kit's detection capability compared to traditional methods.

The first phase of validation sought to determine the specificity of our amplification kit relative to a commercial thermal cycler. For this purpose, four experimental groups were prepared: "pure positive", "pure negative", "dirty positive", and "dirty negative". Each group was processed in triplicate, with one set of reactions amplified using a commercial thermal cycler and the other set amplified using the portable DNA amplification kit presented in this study. Following amplification, impedance analysis revealed that both systems generated distinguishable peak profiles for both negative and positive samples, with distinct and reproducible signatures indicating the presence or absence of DNA nanoballs (Fig. 6(B)). In the negative controls, peak counts remained negligible across both heating systems, confirming that nonspecific amplification did not occur. Meanwhile, in the positive samples, significantly higher peak counts were observed in accordance with the presence of the target DNA. The agreement in peak counts between the two amplification platforms across each sample group demonstrates that our portable device achieves performance parity with established laboratory instrumentation and validates its reliability for the specific amplification of β-lactamase DNA targets. In addition, the variability in the number of detected nanoballs across all four sample groups was considerably lower with our amplification kit, indicating more stable, predictable performance compared to the thermal cycler. The thermal cycler produced higher DNA nanoball counts, but with higher variability, in the pure positive samples. The thermal cycler-derived samples were seemingly more susceptible to matrix effects, with our amplification kit producing fewer but more similar counts of nanoballs across the dirty positive and pure positive samples.

Building on this assessment of specificity, we next examined the sensitivity of the amplification kit through a serial dilution study of dirty positive samples containing increasing concentrations of target β-lactamase DNA (10^1–10^5 copies per μl) and dirty negative samples with 0 copies per μl of target DNA concentration (which translates to replacement of target DNA with nuclease-free water) in the presence of constant background (non-target) mouse DNA. Each sample was run in triplicate, amplified using the DNA amplification kit, and then subjected to impedance-based detection (Fig. 7(A)). The impedance results were compared to qPCR cycle threshold (C_t) values obtained for the same dilutions, providing a rigorous benchmark against the current gold standard (Fig. 7(B)).

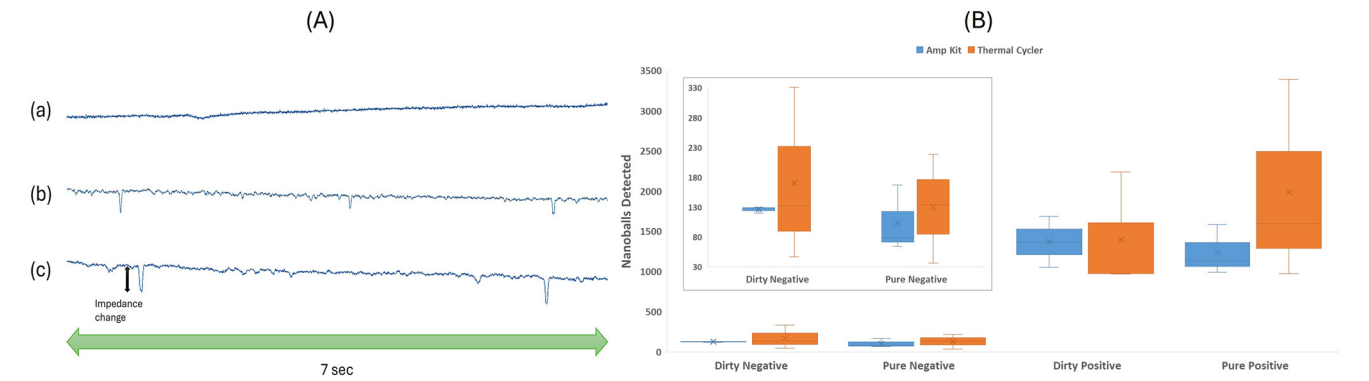

Fig. 6 (A) Randomly selected 7-second window snapshots of the impedance response from the detection system for (a) negative control, (b) portable DNA amplification kit-derived, and (c) thermal cycler-derived samples, showing peaks corresponding to the passage of DNA nanoballs through the impedance-based detection device's microfluidic channel. (B) Box plot of the impedance-based detection of β-lactamase (AMR) nanoballs comparing the response of the dirty and pure pairs of negative control and positive samples, run using either the thermal cycler or our DNA amplification kit. The similarity in peak counts between the two identical reactions, run on either device, indicates successful LAMP reactions facilitated by the DNA amplification kit, demonstrating its ability to compete with traditional, expensive thermal cyclers. As expected, the negative control samples processed by both devices show significantly lower peak counts (around $\frac{1}{10}$) than the positive samples, further validating the accuracy and sensitivity of our amplification reactions. Moreover, the variability in the number of detected nanoballs produced using our amplification kit is much lower than what was amplified using the thermal cycler, particularly when comparing the dirty and pure positive samples.

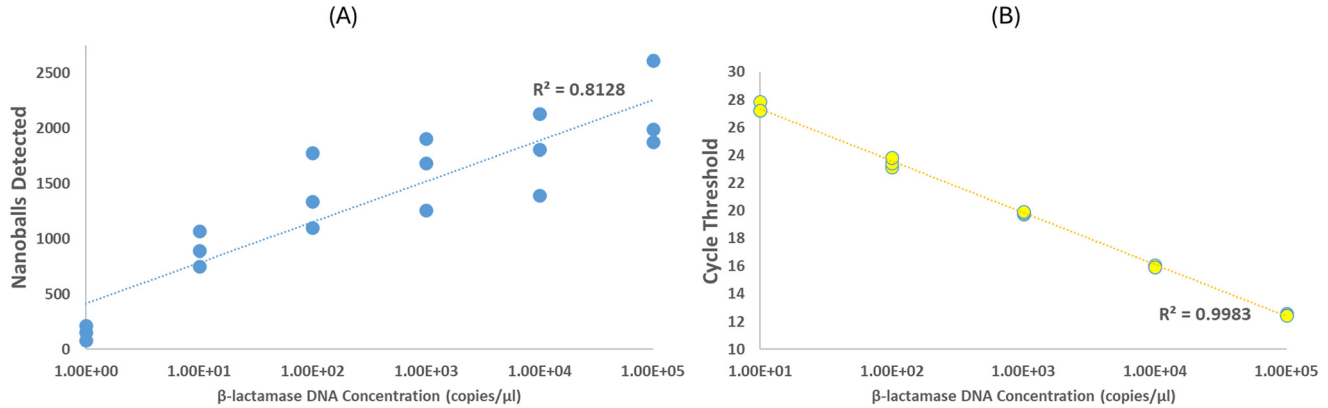

Fig. 7 Results of running the dirty negative and serial dilutions of the dirty positive samples using (A) our DNA amplification kit and microfluidic impedance-based digital assay and (B) standard qPCR approaches. For each approach, a scatter plot showing the (A) peak counts and (B) cycle thresholds from triplicate measurements across dirty negative (0 copies per µl of target DNA) and dirty positive serial dilutions (10^1–10^5 copies per µl of target DNA) is shown. The R^2 value of each plot is presented on the right side. The increasing trendline in nanoball formation and the decreasing trendline in the cycle threshold values demonstrate the quantitative capabilities of the two methods.

C_t values from qPCR are determined based on fluorescent readings taken during the run, in which the fluorescent SYBR dye binds to double-stranded DNA, and as amplification occurs, the amount of double-stranded DNA increases, and therefore, bound SYBR and fluorescence also increase. As these fluorescent values increase, they do so in an exponential manner until reagent limitation causes them to plateau. C_t values can then be calculated by setting a consistent fluorescent value across all samples, and the corresponding cycle number that each reaction was in when meeting this set value can be determined. The lower the C_t value, the fewer cycles it took to reach the set concentration value of DNA, and therefore the higher the starting material concentration; the opposite is true for higher C_t values. The pure samples in the concentration curve and the dirty samples exhibited the same average C_t values, which indicated that the presence of the mouse DNA background did not limit the specificity of the amplification reaction, as the concentration of target DNA remained the same. It should also be noted that the negative samples were not included in the analysis for the qPCR results, as there was no amplification for those samples, as expected, and therefore, there was no corresponding C_t value, but rather the samples served as negative controls for nonspecific amplification.

As expected, both techniques exhibited a clear correlation between target copy number and quantification values: higher DNA concentrations generated high nanoball counts and low C_t values, whereas progressively diluted samples showed fewer nanoballs and correspondingly higher C_t values. Importantly, the amplification kit successfully detected target DNA concentrations down to 10 copies per µL in the reaction (recapitulating the sensitivity observed in the previous study[22]), yielding an average peak count at least sevenfold higher than negative controls (no target DNA [0 copies per µL or dirty negative]). This sensitivity threshold, consistent with prior reports of high-performing isothermal amplification systems, demonstrates that the portable device not only matches qPCR in diagnostic sensitivity but also delivers results without the need for complex thermal cycling instrumentation. It should be noted that the qPCR results had lower variation with an R^2 value of 0.9983, compared to our DNA amplification kit, which had higher variation and an R^2 of 0.8128 (Fig. 7).

Taken together, these findings establish a strong case for the robustness of the DNA amplification kit. The combination of colorimetric detection, impedance-based quantification, and automated induction-heating control enables both rapid preliminary assessment and rigorous quantitative validation within a single workflow. The comparative analyses against both commercial thermal cyclers and qPCR confirm that the system achieves high specificity, avoids false positives in negative controls, and exhibits high sensitivity, reliably detecting target concentrations between 10^1–10^5 copies per µl in the reaction. In doing so, the kit demonstrates performance characteristics that are directly comparable to those of gold-standard laboratory methods, while simultaneously offering a portable, user-friendly, and low-cost alternative optimized for point-of-care and resource-limited environments.

IV. Discussion

The validation experiments and their results described above provide compelling evidence that the portable DNA amplification kit achieves amplification performance comparable to that of conventional thermal cyclers and qPCR, while simultaneously offering distinct advantages in portability, accessibility, and cost-effectiveness. The systematic evaluation of both specificity and sensitivity underscores the robustness of the device and its potential as an innovative tool for de-centralized diagnostics, particularly in contexts where laboratory infrastructure is limited or unavailable. This includes human health-related applications, as described above for AMR or disease monitoring, but can be extended to other fields such as environmental diagnostics. As previously mentioned, using nucleic acids as the target molecule offers flexibility, with customizable primers for the targets of interest, provided the

target regions have a known sequence. This process is important in health contexts with potential high AMR sequence mutational rates, as bacterial immune evasion occurs, but also becomes relevant for systems in which protein or metabolite targets are not well known, such as with understudied environmental systems. This includes but is not limited to: commercial shellfish aquaculture disease monitoring or threatened coral reefs, for which biomarkers of health and disease are still actively being studied, but a low-cost, easily field deployable monitoring system is not yet developed.[36]

One of the most striking outcomes of this study is the high specificity demonstrated across multiple sample conditions, including both pure and complex "dirty" samples containing non-target DNA. The absence of nonspecific amplification in negative control samples heated by the portable kit, together with the close alignment of impedance peak counts with those obtained from a commercial thermal cycler, strongly indicates that the device can reliably discriminate between target and non-target nucleic acids. This is of particular importance for clinical applications, where false positives may lead to inappropriate treatment decisions and contribute to the ongoing challenge of antimicrobial resistance. The validation of specificity in complex backgrounds, such as DNA mixtures, further suggests that the device is well-suited for real-world diagnostic samples that often contain diverse nucleic acid species.

Equally critical is the high sensitivity of the system, as confirmed through direct comparison with qPCR. The ability of the kit to reliably detect as few as 10 target copies per μL in the reaction establishes its utility for early-stage resistance detection, when the number of AMR bacteria may be low, yet clinical intervention is most impactful. The concordance between impedance-based quantification and qPCR cycle thresholds, in addition to the significant R^2 values of the two plots, provides strong validation of the kit's quantitative capability. The higher variability in nanoball counts compared to C_t values indicates that there is room for additional optimization of this approach beyond the prototype presented here. Unlike qPCR, however, the portable kit eliminates the requirement for thermal cycling, optical fluorescence detection, and specialized laboratory settings, making it far more adaptable to decentralized and low-resource environments, potentially overcoming its increased variability. The results of the dilution study also highlight the linear relationship between input target concentration and impedance response, demonstrating that this system is not only qualitative but also capable of providing semi-quantitative or quantitative insights into target DNA abundance.

Beyond the validation experiments, the study highlights several additional advantages inherent to the design of the amplification kit. The visible colorimetric shift provides an immediate and intuitive indicator of amplification success, enabling rapid screening even in the absence of specialized readout devices. The combination of the amplification kit with an impedance-based microfluidic digital assay offers a rigorous secondary confirmation, combining accessibility with quantitative robustness in a single workflow. Furthermore, the engineering innovations that underpin the device, namely the induction heating module, optimized temperature sensor placement, and custom-designed polycarbonate microtube holder, address the challenges faced when designing the amplification kit by ensuring thermal stability, reproducibility, and user safety.

In the broader context of molecular diagnostics, these findings have important implications. By providing a robust alternative and closely competing with the performance of traditional laboratory-based amplification systems, while eliminating their infrastructural demands, the portable DNA amplification kit directly addresses the urgent global need for scalable, decentralized diagnostic tools. This is particularly relevant for the surveillance of antimicrobial resistance (AMR), where rapid and field-deployable detection of resistance genes such as β-lactamase is essential to inform timely therapeutic decision-making and limit the spread of resistant pathogens. More broadly, the platform is adaptable to diverse pathogen targets and can be further integrated into multi-channel or multiplexed diagnostic workflows, offering the potential to expand beyond AMR monitoring into broader infectious disease diagnostics.

Therefore, the DNA amplification kit demonstrates high specificity, high sensitivity, and strong concordance with established gold-standard technologies, confirming its promise as a practical and reliable diagnostic tool. By coupling user-friendly colorimetric quantification with rigorous impedance-based quantification and leveraging low-cost engineering solutions such as induction heating and 3D-printed components, this system bridges the gap between laboratory-grade performance and real-world deployability. Its demonstrated robustness in both controlled and complex sample conditions positions it as a valuable addition to the molecular diagnostic landscape, particularly for point-of-care and resource-limited environments where rapid and accurate detection is most urgently required. Therefore, the next step would be to analyze real patient samples to further establish the amplification kit and become a step closer to an all-in-one, point-of-care AMR diagnostic platform.

V. Conclusion

This research successfully demonstrates the potential of a cost-effective DNA amplification kit designed to combine LAMP with a digital microfluidic impedance-based assay for an all-in-one clinical pathogen detection device at the point-of-care level. By uniting sample processing and detection within one simple workflow, this portable system streamlines molecular diagnostics, reducing operational costs and reagent use, while maintaining high sensitivity and specificity. Through rigorous validation, the device demonstrated high specificity, achieving results indistinguishable from those of a commercial thermal cycler, and high sensitivity, reliably detecting DNA concentrations between 10^1–10^5 copies per μl in the reaction with strong agreement to qPCR standards. The mixture of a

simple visual colorimetric change with a quantitative impedance-based assay provides a dual-layered detection approach that is both accessible and analytically robust. Moreover, the engineering innovations underlying the system, including induction heating, optimized thermocouple placement, and a heat-resistant 3D-printed microtube holder, ensure consistent reaction conditions while maintaining portability and user safety. By bridging the gap between laboratory-grade performance and deployable design, this platform directly addresses critical barriers in global diagnostics. Its demonstrated robustness in complex backgrounds highlights its utility for real-world clinical samples, particularly in antimicrobial resistance detection, where rapid, field-deployable solutions are urgently needed. Moving forward, this system holds promise as a scalable, adaptable tool in rapid diagnostics, especially relevant for monitoring antimicrobial resistance and infectious disease control in clinical and remote applications. This two-stage system can be further upgraded into a multi-channel lab-on-chip capable of simultaneously detecting several pathogens from a single test.

Conflicts of interest

The authors have no conflicts to disclose.

Data availability

The data supporting this article have been included as part of the supplementary information (SI). Supplementary information: SI contains the raw and processed experimental data supporting this study, including impedance peak values and counts from the microfluidic digital assay, qPCR cycle threshold (C_t) values, replicate measurements, and statistical analyses used to generate the figures and validate system performance. See DOI: https://doi.org/10.1039/d6lc00062b.

Acknowledgements

This research was funded by the National Science Foundation grant number 1846740 awarded to Mehdi Javanmard and Catalyst Science Fund, Revive & Restore, awarded to Debashish Bhattacharya and Mehdi Javanmard. This work was also supported by grants from the National Science Foundation (2128073), The Nature Conservancy, and the USDA National Institute of Food and Agriculture Hatch Formula (NJ01180) awarded to Debashish Bhattacharya. Vicent Pelechano acknowledges support from the Swedish Research Council (VR 2022-05272, VR 2023-02026) and the Knut and Alice Wallenberg Foundation [WAF2021.0167].

References

1 C. J. L. Murray, K. S. Ikuta, F. Sharara, L. Swetschinski, G. R. Aguilar and A. Gray, *et al.*, Global burden of bacterial antimicrobial resistance in 2019: a systematic analysis, *Lancet*, 2022, **399**(10325), 629–655, DOI: 10.1016/s0140-6736(21)02724-0.

2 A. Vasala, V. P. Hytönen and O. H. Laitinen, Modern Tools for Rapid Diagnostics of Antimicrobial Resistance, *Front. Cell. Infect. Microbiol.*, 2020, **10**, 308, DOI: 10.3389/fcimb.2020.00308.

3 J. Hassall, C. Coxon, V. C. Patel, S. D. Goldenberg and C. Sergaki, Limitations of current techniques in clinical antimicrobial resistance diagnosis: examples and future prospects, *npj Antimicrob. Resist.*, 2024, **2**(1), 16, DOI: 10.1038/s44259-024-00033-8.

4 M. N. Esbin, O. N. Whitney, S. Chong, A. Maurer, X. Darzacq and R. Tjian, Overcoming the bottleneck to widespread testing: a rapid review of nucleic acid testing approaches for COVID-19 detection, *RNA*, 2020, **26**(7), 771–783, DOI: 10.1261/rna.076232.120.

5 B. T. Teoh, S. S. Sam and K. K. Tan, *et al.* Detection of dengue viruses using reverse transcription-loop-mediated isothermal amplification, *BMC Infect. Dis.*, 2013, **13**, 387, DOI: 10.1186/1471-2334-13-387.

6 L. Yan, J. Zhou, Y. Zheng, A. S. Gamson, B. T. Roembke and S. Nakayama, *et al.* Isothermal amplified detection of DNA and RNA, *Mol. BioSyst.*, 2014, **10**, 970–1003, DOI: 10.1039/C3MB70304E.

7 A. Alekseenko, D. Barrett and Y. Pareja-Sanchez, *et al.* Direct detection of SARS-CoV-2 using non-commercial RT-LAMP reagents on heat-inactivated samples, *Sci. Rep.*, 2021, **11**, 1820, DOI: 10.1038/s41598-020-80352-8.

8 M. Sasano, M. Seki, C. Takano, S. Komine-Aizawa and S. Hayakawa, An improved primer design for the loop-mediated isothermal amplification (LAMP) method to detect oxacillinase (OXA)-48-lactamase genes in Gram-negative bacteria for clinical applications, *J. Infect. Chemother.*, 2021, **27**(7), 1005–1012, Available from: https://www.sciencedirect.com/science/article/pii/S1341321X21000568.

9 E. Tacconelli, E. Carrara, A. Savoldi, S. Harbarth, M. Mendelson and D. L. Monnet, *et al.* Discovery, research, and development of new antibiotics: the WHO priority list of antibiotic-resistant bacteria and tuberculosis, *Lancet Infect. Dis.*, 2017, **18**(3), 318–327, DOI: 10.1016/s1473-3099(17)30753-3.

10 D. M. Livermore and N. Woodford, The -lactamase threat in Enterobacteriaceae, Pseudomonas and Acinetobacter, *Trends Microbiol.*, 2006, **14**(9), 413–420, DOI: 10.1016/j.tim.2006.07.008.

11 H. Zhang, Y. Xu, Z. Fohlerova, H. Chang, C. Iliescu and P. Neuzil, LAMP-on-a-chip: Revising microfluidic platforms for loop-mediated DNA amplification, *TrAC, Trends Anal. Chem.*, 2019, **113**, 44–53, Available from: https://www.sciencedirect.com/science/article/pii/S0165993618307015.

12 J. Compton, Nucleic acid sequence-based amplification, *Nature*, 1991, **350**(6313), 91–92, Available from: https://www.nature.com/articles/350091a0#citeas.

13 A. Toldrà, M. Jauset-Rubio, K. B. Andree, M. Fernández-Tejedor, J. Diogène and I. Katakis, *et al.* Detection and quantification of the toxic marine microalgae Karlodinium veneficum and Karlodinium armiger using recombinase polymerase amplification and enzyme-linked oligonucleotide assay, *Anal. Chim. Acta*, 2018, **1039**, 140–148, Available from: https://www.sciencedirect.com/science/article/pii/S0003267018309218.

14 M. Vincent, Y. Xu and H. Kong, Helicase-dependent isothermal DNA amplification, *EMBO Rep.*, 2004, **5**(8), 795–800, DOI: 10.1038/sj.embor.7400200.

15 T. Notomi, H. Okayama, H. Masubuchi, T. Yonekawa, K. Watanabe and N. Amino, *et al.* Loop-mediated isothermal amplification of DNA, *Nucleic Acids Res.*, 2000, **28**(12), 63e–663, Available from: https://pubmed.ncbi.nlm.nih.gov/10871386/.

16 K. J. M. Moore, J. Cahill, G. Aidelberg, R. Aronoff, A. Bektas and D. Bezdan, *et al.* Loop-Mediated isothermal amplification detection of SARS-COV-2 and myriad other applications, *J. Biomol. Tech.*, 2021, **32**(3), 228–275, DOI: 10.7171/jbt.21-3203-017.

17 M. Zhang, J. Ye, J. Song He, F. Zhang, J. Ping and C. Qian, *et al.* Visual detection for nucleic acid-based techniques as potential on-site detection methods. A review, *Anal. Chim. Acta*, 2020, **1099**, 1–15, Available from: https://www.sciencedirect.com/science/article/pii/S0003267019314199.

18 M. Nagura-Ikeda, K. Imai, S. Tabata, K. Miyoshi, N. Murahara, T. Mizuno, M. Horiuchi, K. Kato, Y. Imoto, M. Iwata, S. Mimura, T. Ito, K. Tamura and Y. Kato, Clinical Evaluation of Self-Collected Saliva by Quantitative Reverse Transcription-PCR (RT-qPCR), Direct RT-qPCR, Reverse Transcription–Loop-Mediated Isothermal Amplification, and a Rapid Antigen Test To Diagnose COVID-19, *J. Clin. Microbiol.*, 2020, **58**(9), DOI: 10.1128/jcm.01438-20.

19 R. R. G. Soares, A. S. Akhtar, I. F. Pinto, N. Lapins, D. Barrett and G. Sandh, *et al.* Sample-to-answer COVID-19 nucleic acid testing using a low-cost centrifugal microfluidic platform with bead-based signal enhancement and smartphone read-out, *Lab Chip*, 2021, **21**, 2932–2944, DOI: 10.1039/D1LC00266J.

20 S. M. DeFina, J. Wang and L. Yang, *et al.* SaliVISION: a rapid saliva-based COVID-19 screening and diagnostic test with high sensitivity and specificity, *Sci. Rep.*, 2022, **12**, 5729, DOI: 10.1038/s41598-022-09718-4.

21 Q. Yang, N. R. Meyerson, S. K. Clark, C. L. Paige, W. T. Fattor, A. R. Gilchrist, A. Barbachano-Guerrero, B. G. Healy, E. R. Worden-Sapper, S. S. Wu, D. Muhlrad, C. J. Decker, T. K. Saldi, E. Lasda, P. Gonzales, M. R. Fink, K. L. Tat, C. R. Hager, J. C. Davis, C. D. Ozeroff, G. R. Brisson, M. B. McQueen, L. A. Leinwand, R. Parker and S. L. Sawyer, Saliva TwoStep for rapid detection of asymptomatic SARS-CoV-2 carriers, *eLife*, 2021, **10**, e65113, DOI: 10.7554/elife.65113.

22 M. Tayyab, D. Barrett, G. van Riel, S. Liu, B. Reinius and C. Scharfe, *et al.* Digital assay for rapid electronic quantification of clinical pathogens using DNA nanoballs, *Sci. Adv.*, 2023, **9**(36), eadi4997, DOI: 10.1126/sciadv.adi4997.

23 F. Lisdat and D. Schäfer, The use of electrochemical impedance spectroscopy for biosensing, *Anal. Bioanal. Chem.*, 2008, **391**(5), 1555–1567, DOI: 10.1007/s00216-008-1970-7.

24 L. Becherer, N. Borst, M. Bakheit, S. Frischmann, R. Zengerle and F. von Stetten, Loop-mediated isothermal amplification (LAMP) – review and classification of methods for sequence-specific detection, *Anal. Methods*, 2020, **12**, 717–746, DOI: 10.1039/C9AY02246E.

25 O. Lucía, P. Maussion, E. J. Dede and J. M. Burdío, Induction Heating Technology and Its Applications: Past Developments, Current Technology, and Future Challenges, *IEEE Trans. Ind. Electron. Control Instrum.*, 2014, **61**(5), 2509–2520.

26 R. Lenhard, M. Malcho and K. Kaduchová, Numerical simulation of induction heating thick-walled tubes, *MATEC Web Conf.*, 2018, **168**, 02004, DOI: 10.1051/matecconf/201816802004.

27 S. Farah, D. G. Anderson and R. Langer, Physical and mechanical properties of PLA, and their functions in widespread applications — A comprehensive review, *Adv. Drug Delivery Rev.*, 2016, **107**, 367–392, PLA biodegradable polymers. Available from: https://www.sciencedirect.com/science/article/pii/S0169409X16302058.

28 C. Benwood, A. Anstey, J. Andrzejewski, M. Misra and A. K. Mohanty, Improving the Impact Strength and Heat Resistance of 3D Printed Models: Structure, Property, and Processing Correlationships during Fused Deposition Modeling (FDM) of Poly(Lactic Acid), *ACS Omega*, 2018, **3**(4), 4400–4411, DOI: 10.1021/acsomega.8b00129, PMID: 31458666.

29 M. Grasso, L. Azzouz, P. Ruiz-Hincapie, M. Zarrelli and G. Ren, Effect of temperature on the mechanical properties of 3D-printed PLA tensile specimens, *Rapid Prototyp. J.*, 2018, **24**(8), 1337–1346, DOI: 10.1108/rpj-04-2017-0055.

30 M. H. Hsueh, C. J. Lai, S. H. Wang, Y. S. Zeng, C. H. Hsieh and C. Y. Pan, *et al.* Effect of printing parameters on the thermal and mechanical properties of 3D-Printed PLA and PETG, using fused deposition modeling, *Polymer*, 2021, **13**(11), 1758, DOI: 10.3390/polym13111758.

31 A. a. B. A. Bakar, M. Z. B. Zainuddin, A. N. B. Adam, I. S. B. M. Noor, N. B. Tamchek, M. S. B. Alauddin and M. I. B. M. Ghazali, The study of mechanical properties of poly(lactic) acid PLA-based 3D printed filament under temperature and environmental conditions, *Mater. Today: Proc.*, 2022, **67**, 652–658, DOI: 10.1016/j.matpr.2022.06.198.

32 N. Jayanth, K. Jaswanthraj, S. Sandeep, N. H. Mallaya and S. R. Siddharth, Effect of heat treatment on mechanical properties of 3D printed PLA, *J. Mech. Behav. Biomed. Mater.*, 2021, **123**, 104764, Available from: https://www.sciencedirect.com/science/article/pii/S1751616121004070.

33 Y. Ho Kim, I. Yang, Y.-S. Bae and S.-R. Park, Performance Evaluation of Thermal Cyclers for PCR in a Rapid Cycling Condition, *BioTechniques*, 2008, **44**(4), 495–505, DOI: 10.2144/000112705.

34 Thermocyclers — Thermo Fisher Scientific – US, Available from: https://www.thermofisher.com/thermalcyclers.

35 K. Karimi, A. Fardoost, N. Mhatre, J. Rajan, D. Boisvert and M. Javanmard, A thorough review of emerging technologies in micro-and nanochannel fabrication: limitations, applications, and comparison, *Micromachines*, 2024, **15**(10), 1274, DOI: 10.3390/mi15101274.

36 E. E. Chille, T. G. Stephens, S. Nandi, H. Jiang, M. J. Gerdes and O. M. Williamson, *et al.* Coral Restoration in the Omics Era: Development of Point-of-Care Tools for Monitoring Disease, Reproduction, and Thermal Stress, *BioEssays*, 2025, e70007, forthcoming.